



Gravitational signature of Jupiter's internal dynamics

Yohai Kaspi,¹ William B. Hubbard,² Adam P. Showman,² and Glenn R. Flierl³

Received 19 October 2009; revised 19 November 2009; accepted 7 December 2009; published 15 January 2010.

[1] Telescopic observations and space missions to Jupiter have provided vast information about Jupiter's cloud level winds, but the depth to which these winds penetrate has remained an ongoing mystery. Scheduled to be launched in 2011, the Jupiter orbiter *Juno* will make high-resolution observations of Jupiter's gravity field. In this paper we show that these measurements are sensitive to the depth of the internal winds. We use dynamical models ranging from an idealized thermal wind balance analysis, using the observed cloud-top winds, to a full general circulation model (GCM). We relate the depth of the dynamics to the external gravity spectrum for different internal wind structure scenarios. In particular, we predict that substantial Jovian winds below a depth of 500 km would lead to detectable (milligal-level) gravity anomalies with respect to the expected gravity for a planet in solid body rotation. **Citation:** Kaspi, Y., W. B. Hubbard, A. P. Showman, and G. R. Flierl (2010), Gravitational signature of Jupiter's internal dynamics, *Geophys. Res. Lett.*, 37, L01204, doi:10.1029/2009GL041385.

1. Introduction

[2] To date, direct observational data on the circulation of giant planets has been limited to atmospheric layers whose cloud motions can be tracked at optical and infrared wavelengths, and to in situ Jupiter measurements carried out by the 1995 Galileo Entry Probe (GEP). Here we show that high-precision measurements of Jupiter's external gravity field can be used to probe the dynamics of much deeper layers. The GEP entered a low-latitude region in Jupiter where cloud motions show strong eastward wind speeds of $\sim 80 \text{ m s}^{-1}$ with respect to Jupiter's magnetic-field-stationary frame. At deepest penetration (22 bars, and only 0.2% of the planetary radius), the GEP measured wind speeds approaching 160 m s^{-1} [Atkinson *et al.*, 1996]. We do not know whether such zonal jets on Jupiter extend to much higher pressures (and therefore involve significant planetary mass) or if they disappear at greater depths (see Vasavada and Showman [2005] for a review). Due to Jupiter's internal heat source and rapid rotation it has been suggested [Busse, 1976; Ingersoll and Pollard, 1982] that the observed surface zonal flows on Jupiter extend to the interior along cylinders parallel to the axis of rotation. Recent studies have shown that the interior flow, which can be driven by internal or surface forcing [Showman *et al.*, 2006; Lian and

Showman, 2008], should have a radial shear resulting in weaker interior winds due to both compressible effects [Kaspi *et al.*, 2009] and ohmic dissipation [Liu *et al.*, 2008; Schneider and Liu, 2009].

[3] How do the winds affect the gravity signature? The spectrum of the gravity harmonics is determined by the planetary mass distribution. Low-degree zonal harmonics of a planet like Jupiter are mostly produced by the oblateness caused by bulk rotation. However, just as on Earth, winds are associated with atmospheric high and low pressures (and therefore with density anomalies with respect to the mean air density), and we expect Jupiter's winds to likewise induce density anomalies that affect the mass distribution. Unlike terrestrial planets, giant planet atmospheres contain a more significant fraction of the total mass and therefore the effect of the winds can be measured even though these measurements will still have far less resolution than the comparable measurements for terrestrial planets [e.g., Tapley *et al.*, 2004; Smith *et al.*, 2001]. *Juno* will make the first such measurements on giant planets. We show that beyond the tenth-degree zonal gravity harmonic (potentially measurable by *Juno*), dynamically-driven harmonics become stronger than the gravity harmonics of a quiescent Jupiter (rotating as a solid body). Effects of these high-order harmonics on the external gravity can be measured and used to indicate the existence of deep winds.

[4] The gravity at any external point \mathbf{r} to Jupiter is given by $\mathbf{g}(\mathbf{r}) = \nabla V$ where V is the gravitational potential. Since to leading order the dynamics on Jupiter are zonally symmetric, we focus in this study on the zonally symmetric gravity response to the dynamics. The axially-symmetric gravitational potential can be expanded in terms of Legendre Polynomials (P_n) so that

$$V(\mathbf{r}) = \frac{GM}{r} \left[1 - \sum_{n=2}^{\infty} \left(\frac{a}{r} \right)^n J_n P_n(\mu) \right], \quad (1)$$

where G is the gravitational constant, M is the planetary mass, $a \approx 7 \times 10^4 \text{ km}$ is the planetary radius, \mathbf{r} is the vector position of the point of observation from the planet's center of mass; \mathbf{r} has length r and points toward colatitude θ measured from Jupiter's rotation axis ($\mu = \cos\theta$) [Hubbard, 1984]. The zonal harmonics J_n are weighted integrals over Jupiter's interior mass distribution and are given by

$$J_n = -\frac{1}{Ma^n} \int_0^a r'^{2+n} dr' \int_0^{2\pi} d\phi' \int_{-1}^1 P_n(\mu') \rho(r', \mu', \phi') d\mu'. \quad (2)$$

Since (2) is linear in the density distribution $\rho(\mathbf{r})$, we may replace $\rho(\mathbf{r})$ in equation (2) with density anomalies $\rho'(\mathbf{r})$ defined with respect to an unperturbed hydrostatic radial density distribution $\bar{\rho}(r)$, and then calculate the contribution

¹Division of Geological and Planetary Sciences, California Institute of Technology, Pasadena, California, USA.

²Lunar and Planetary Laboratory, University of Arizona, Tucson, Arizona, USA.

³Department of Earth, Atmospheric, and Planetary Sciences, Massachusetts Institute of Technology, Cambridge, Massachusetts, USA.

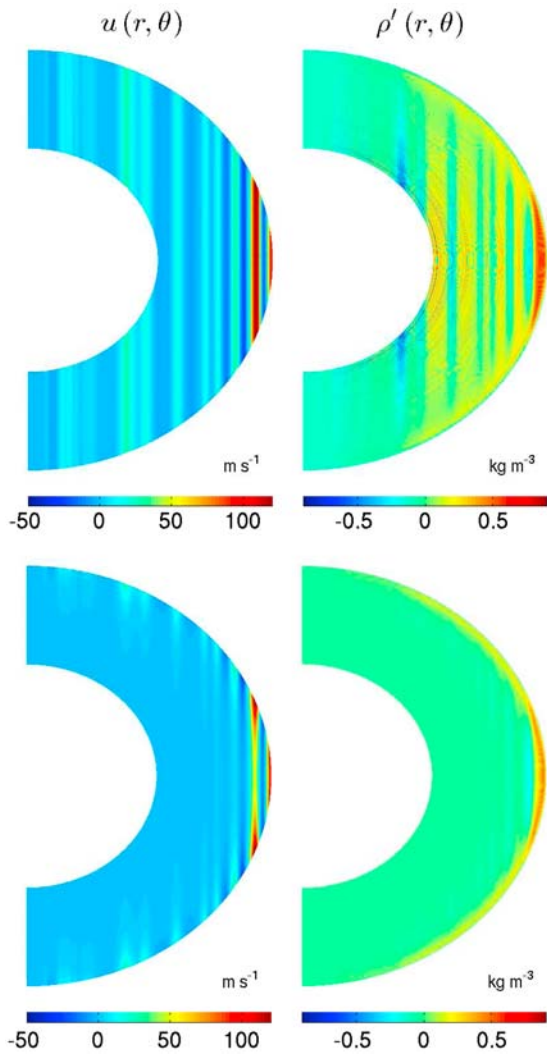


Figure 1. Examples of the idealized zonal velocity fields (left) for cases of $H = 10^8$ km (top) and $H = 5000$ km (bottom), with northern hemisphere winds and the resulting density anomaly field (right) calculated by thermal wind balance (equation (3)).

of density anomalies alone to the multipole coefficients. We denote these contributions by ΔJ_n . Therefore given the density anomalies due to the winds relative to the planet at a rest state, we can calculate the gravity moment anomalies ΔJ_n that result from these winds.

[5] The first investigation of Jupiter's dynamics-related gravity anomalies was carried out by Hubbard [1999, hereafter H99]. H99 did not simulate Jupiter's interior dynamics, as we do here, but merely investigated the consequences of mapping Jupiter's observed zonal winds onto differentially-rotating cylinders with the axis of each cylinder coinciding with Jupiter's angular-momentum vector, assuming a generalized hydrostatic state. H99 showed for this model that the predicted gravity-harmonic spectrum for a Jupiter in solid-body rotation, with even gravitational harmonics only, would decrease geometrically with respect to n , with signs alternating as $(-1)^{1+n/2}$. After including the effects of zonal winds mapped onto cylinders, the high

order harmonics go to a less regular, saturated pattern. Interior models for Jupiter derived from a first-principles equation of state [Militzer *et al.*, 2008] could not be matched to Jupiter's fourth-order gravity harmonic J_4 except by invoking interior dynamics. This result implied that the signature of Jovian interior dynamics might appear even at degree four. In the case of Neptune, we know that the value of that planet's J_4 requires that strong retrograde equatorial winds are confined to the outermost few percent of the planetary mass [Hubbard *et al.*, 1991]. No comparable constraints yet exist for Jupiter. Answering this question is a major goal of the *Juno* mission.

2. Models

[6] In order to study the relation between the velocity field and the resulting gravity harmonics we use two independent models. For the first and simpler one, we impose the cloud level winds from observations [Limaye, 1986; Porco *et al.*, 2003] and construct a hypothetical interior velocity structure which we systematically vary to study its effect on the gravity signature. We therefore use the observed winds and extend these parallel to the axis of rotation (symmetrically across the equator with either a northern or southern hemisphere wind profile), with a vertical decay function crudely intended to parameterize the decay shown by Kaspi *et al.* [2009] or Liu *et al.* [2008]. Then the zonal wind is $u(r, \theta) = u_{cyl} e^{-\frac{r}{H}}$, where $u_{cyl}(r, \theta)$ is a function that extends the cloud level winds constant along the direction of the axis of rotation, and H is the e-folding depth of the cloud level winds. The e-folding depth H is a free parameter, and varying it systematically allows studying the dependence of the gravity harmonics on the vertical extent of the winds. Thus when $H \gg a$ the zonal wind is nearly constant along the direction of the axis of rotation and as H decreases the zonal velocity decreases with depth.

[7] The rapid rotation and large scale of the planet imply that to the leading order the planet is in geostrophic balance, and therefore the thermal wind relation must hold so that

$$(2\Omega \cdot \nabla)[\tilde{\rho}\mathbf{u}] = \nabla\rho' \times \mathbf{g}_0, \quad (3)$$

where Ω is the planetary rotation vector, $\tilde{\rho}(r)$ is the basic hydrostatic state density, $\mathbf{u}(\mathbf{r})$ is the full 3D velocity, $\mathbf{g}_0(r)$ is the mean gravity vector and $\rho'(\mathbf{r})$ is the density anomaly [Pedlosky, 1987; Kaspi *et al.*, 2009]. Thus given the vertical mean density structure (which is known from 1D structure models [Guillot and Morel, 1995]), and the zonal wind profile the thermal wind relation can be integrated to calculate the density anomaly resulting from the dynamics. This method is demonstrated in Figure 1 which shows the axisymmetric zonal wind profile on a meridional slice through the planet for two cases: The upper panels correspond to a case with $H = 10^8$ km, and thus no decay in velocity along the direction of the axis of rotation, and the lower panels show a case with $H = 5000$ km, having the same cloud top winds but interior flows which decay exponentially with an e-folding depth of 5000 km. Both cases are characterized by a positive density anomaly near the equatorial eastward flow (superrotation) region, though for the $H = 5000$ km case this anomaly is weaker. For this

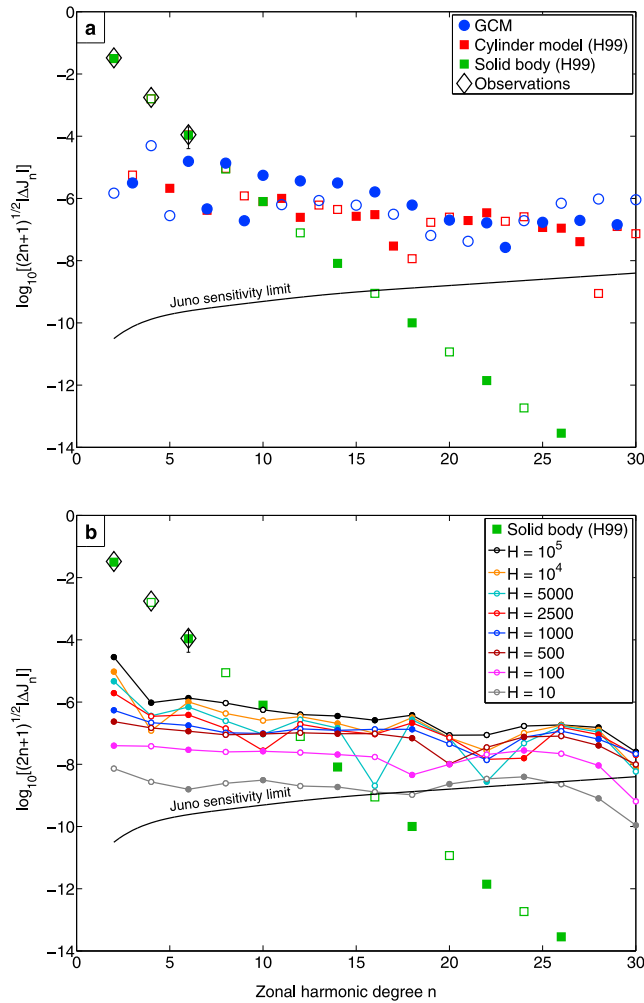


Figure 2. (a) The zonal gravity harmonics (ΔJ_n) for the GCM, and H99's rotation on cylinders model averaged over hemispheres. Green squares give J_n for the solid body model of H99. Filled (open) symbols refer to positive (negative) harmonics. (b) The even zonal gravity harmonics resulting from the dynamics (ΔJ_n) for cases of different zonal velocity scale heights (H) using the idealized thermal wind model.

calculation we use a northern hemisphere wind profile, an interior mean density profile $\bar{\rho}(r)$ which varies from 0.16 to 2200 kg m^{-3} [Kaspi et al., 2009; Guillot and Morel, 1995], and a mean gravity field $\mathbf{g}_0(r)$ calculated by integrating $\bar{\rho}(r)$.

[8] The second model we use to calculate the density anomaly resulting from the dynamics is a full 3D non-hydrostatic anelastic general circulation model [Kaspi, 2008] which is driven by internal heat, has an equation of state for high pressure hydrogen (SCVH) [Saumon et al., 1995], and has realistic vertical structure of the basic (no winds) state density, temperature, gravitational acceleration, thermal expansion and compressibility. The vertical structure is calculated assuming an adiabatic and hydrostatic reference state and the SCVH equation of state. It matches well with other estimates of the internal thermodynamical structure of the planet [Guillot and Morel, 1995]. Here the 3D density anomaly is calculated dynamically in the model, and can be used directly for the gravity harmonics calcula-

tion. The advantage of this model is that it has a better internal thermodynamical structure and has a representation of the convection driving the system. However, although reproducing the main features of the dynamics such as the equatorial superrotation it does not reproduce the complete observed cloud level winds and therefore a comparison against the first model and the potential theory model of H99 is required.

3. Results

[9] Taking the dynamical density fields from the two models, we can use equation (2) to calculate the resulting gravity harmonics; these are shown in Figures 2a and 2b. Filled symbols represent positive values of J_n and open symbols represent negative values. We compare these to a reference Jupiter rotating as a solid body at a fixed angular rotation rate Ω , shown here by the green squares calculated analytically for a polytrope of index one (H99). In hydrostatic equilibrium the reference Jupiter's spectrum of zonal harmonics has the previously-described character (only even values of J_n , with alternating signs, and a geometric decrease with n). Diamonds show the observed Jovian values [Campbell and Synnott, 1985], with the error bar on J_6 the only discernible error bar on this plot.

[10] Figures 2a and 2b show that beyond J_{10} the contribution of the dynamical part of the gravity harmonics is larger than the solid-body part for both the GCM and the idealized model. The amplitudes of the harmonics are similar to those of H99, but not identical mostly because in H99 it was assumed that the mean density $\bar{\rho}$ is a polytrope of index one while here we use a more realistic profile calculated using the SCVH equation of state. The larger values of the even harmonics are due to the high degree of north-south symmetry in the GCM simulations. The black line shows the estimate for the sensitivity of the *Juno* gravity experiment (J. D. Anderson, personal communication, 2009). The lower J_n are dominated by contributions from the oblate shape of the planet. We do not take into account global distortions from spherical symmetry in our idealized model or the GCM, which compute dynamical density anomalies with respect to a spherical hydrostatic density distribution and which therefore give only the dynamical part (ΔJ_n). The low-degree harmonics are sensitive not only to the equation of state but also to the mass and density of a heavy-element core, which is not included in the model. Therefore, we have not added the hydrostatic contributions but have focused on the higher harmonics for which the signals from the dynamical model are orders of magnitude larger than those from the oblateness.

[11] The effect of deep circulation on the dynamics is analyzed by looking at cases where the interior winds decay with depth and thus $H \ll a$. If the interior velocities become weaker with depth then so will the resulting density anomalies. This is shown in Figure 2b where we plot the averaged northern and southern hemisphere gravity harmonics for cases of different H values using the idealized model. This calculation predicts that if the velocity is constant along cylinders then for all $n \geq 10$ the ΔJ_n should be greater than or comparable in absolute value to the solid body J_n ; if the e-folding depth of the decay in zonal wind is greater than 500 km then ΔJ_{12} and beyond should be greater than the

solid body value. If the winds decay more rapidly with depth, then the anomaly due to the winds would only appear in ΔJ_{14} . This is shown explicitly in Figure 3 where we compare the average northern and southern hemisphere harmonics to the solid body contribution for the first three harmonics where the effects of the dynamics are detectable (J_{10} , J_{12} and J_{14}). Note that even if the value due to the dynamics is smaller than the solid-body value, ΔJ_n may still be detectable by comparing the observed J_n with theoretical values.

[12] Of particular importance is J_4 since there is a discrepancy between the observed value of J_4 and that obtained by interior structure models such as *Militer et al.* [2008] which requires a contribution of $\Delta J_4 \approx 3 \times 10^{-5}$ from the dynamics to bring the model to agreement with observations. We find that although our correction to J_4 is in the right direction (positive), its maximum value is only $\Delta J_4 \approx 8 \times 10^{-7}$ and thus too weak. In order to match this discrepancy interior winds would have to increase by a factor of 30 compared to the cloud top winds which is unrealistic. Therefore we conclude that dynamics alone cannot explain the discrepancy in J_4 .

[13] Another way of detecting the gravity signature of the dynamics is to look directly at spatially varying gravity anomalies as measured by the orbiter, rather than the gravity harmonics spectrum derived from a fit to spacecraft accelerations. In Figure 4a we show the dynamically induced gravity anomalies calculated from the GCM, the idealized model, and from the H99 model. Recognizing that *Juno* will not measure accelerations as close to Jupiter as $r = a$, but at distances (near periapse) of, say, $r = a + 5000$ km we perform the calculations at that distance. All three models predict a maximum corresponding to the positive density anomaly near the equatorial superrotating region (Figure 1), with values of more than 50 mgal referenced to Jupiter rotating as a solid body.

[14] Since there is no way to experimentally separate the dynamic and solid body contributions to the low harmonics, and since all three models predict that dynamics will dominate the gravity spectrum above degree ten, a possible analysis approach would be to use *Juno* data to obtain a symmetric best-fit model with even zonal harmonics of

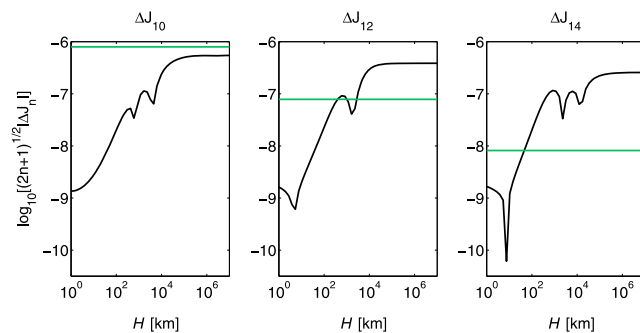


Figure 3. The first three even zonal harmonics where the contribution from the dynamics (black) is comparable or greater than the solid body harmonics (green) as a function of the e-folding depth of the winds (H). The green and black lines intersect at the depth where the contribution from the dynamics (ΔJ_n) becomes greater than the contribution from the planet at rest (J_n).

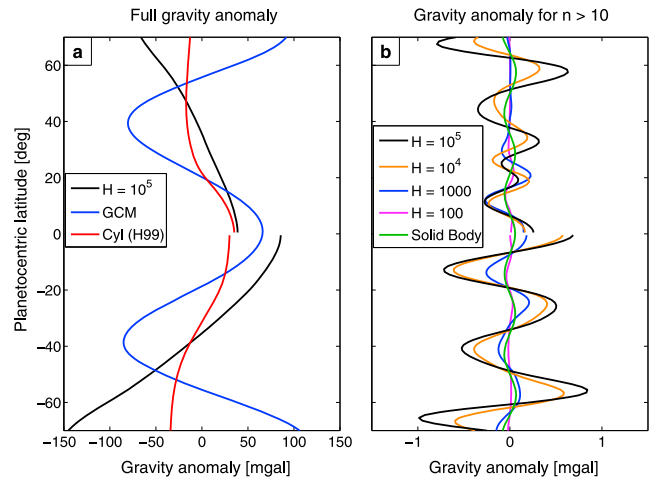


Figure 4. The gravity anomaly (mgal) calculated at 5000 km above the cloud top level as function of latitude. (a) The dynamically induced gravity anomaly for the idealized model with $H = 10^5$ km, the GCM and the rotation on cylinders model of H99. (b) The gravity anomaly from contributions beyond the 10th degree for different vertical structures in the idealized model compared to the solid body contribution. Colors match those of Figure 2.

degree ten and below. Gravity residuals with respect to this model, which may include significant contributions from low-degree north-south asymmetric terms such as J_3 , J_5 etc., would be clearly attributable to dynamics. Figure 4b shows a simulation of this procedure for cases of $H = 10^5$, 10^4 , 1000 and 10 km, where gravity anomalies with respect to a north-south-symmetric tenth-degree reference field are predicted to have a peak-to-peak amplitude of order 1 mgal (compared to 0.2 mgal for a quiescent Jupiter). Given that the instrumental design limit for the *Juno* gravity experiment is 1 to 10 μ gal, mgal-level gravity anomalies with respect to a best-fit tenth-degree Jovian gravity field should be readily detectable. Thus, a careful determination of gravity anomalies in *Juno* acceleration data may give a robust confirmation of deep-seated dynamics in Jupiter. Moreover, these results imply that even if the winds on Jupiter are quite shallow (on the order of a few hundred km which are less than 1% of the radius of the planet) they still should produce a signal which will be measurable by *Juno*.

[15] **Acknowledgments.** We thank Andrew Ingersoll, Tapio Schneider, David Stevenson, and two anonymous reviewers for their comments and suggestions. This research has been supported by NSF grant AST-0708106 (Y.K., A.S. and G.F.), NASA grant NNX07AF35G (A.S.), the NOAA Climate and Global Change Postdoctoral Fellowship administered by the University Corporation for Atmospheric Research. (Y.K.) and the *Juno* project (W.H.).

References

- Atkinson, D. H., J. B. Pollack, and A. Seiff (1996), Galileo Doppler measurements of the deep zonal winds at Jupiter, *Science*, 272, 842–843.
- Busse, F. H. (1976), A simple model of convection in the Jovian atmosphere, *Icarus*, 29, 255–260.
- Campbell, J. K., and S. P. Synnott (1985), Gravity field of the Jovian system from Pioneer and Voyager tracking data, *Astrophys. J.*, 90, 364–372.
- Guillot, T., and P. Morel (1995), CEPAM: A code for modeling the interiors of giant planets, *Astron. Astrophys.*, 109, 109–123.

- Hubbard, W. B. (1984), *Planetary Interiors*, 343 pp., Van Nostrand Reinhold, New York.
- Hubbard, W. B. (1999), Gravitational signature of Jupiter's deep zonal flows, *Icarus*, *137*, 357–359.
- Hubbard, W. B., W. J. Nellis, A. C. Mitchell, N. C. Holmes, P. C. McCandless, and S. S. Limaye (1991), Interior structure of Neptune—Comparison with Uranus, *Science*, *253*, 648–651.
- Ingersoll, A. P., and D. Pollard (1982), Motion in the interiors and atmospheres of Jupiter and Saturn: Scale analysis, anelastic equations, barotropic stability criterion, *Icarus*, *52*, 62–80.
- Kaspi, Y. (2008), Turbulent convection in rotating anelastic spheres: A model for the circulation on the giant planets, Ph.D. thesis, Mass. Inst. of Technol., Cambridge.
- Kaspi, Y., G. R. Flierl, and A. P. Showman (2009), The deep wind structure of the giant planets: Results from an anelastic general circulation model, *Icarus*, *202*, 525–542.
- Lian, Y., and A. P. Showman (2008), Deep jets on gas-giant planets, *Icarus*, *194*, 597–615.
- Limaye, S. S. (1986), Jupiter: New estimates of mean zonal flow at the cloud level, in *Jovian Atmospheres*, edited by M. Allison and L. D. Travis, *NASA Conf. Publ.*, *2441*, 124–128.
- Liu, J., P. M. Goldreich, and D. J. Stevenson (2008), Constraints on deep-seated zonal winds inside Jupiter and Saturn, *Icarus*, *196*, 653–664.
- Militzer, B., W. B. Hubbard, J. Vorberger, I. Tamblyn, and S. A. Boney (2008), A massive core in Jupiter predicted from first-principles simulations, *Astrophys. J.*, *688*, L45–L48.
- Pedlosky, J. (1987), *Geophysical Fluid Dynamics*, Springer, New York.
- Porco, C. C., et al. (2003), Cassini imaging of Jupiter's atmosphere, satellites and rings, *Science*, *299*, 1541–1547.
- Saumon, D., G. Chabrier, and H. M. van Horn (1995), An equation of state for low-mass stars and giant planets, *Astrophys. J.*, *99*, 713.
- Schneider, T., and J. J. Liu (2009), Formation of jets and equatorial super-rotation on Jupiter, *J. Atmos. Sci.*, *66*, 579–601.
- Showman, A. P., P. J. Gierasch, and Y. Lian (2006), Deep zonal winds can result from shallow driving in a giant-planet atmosphere, *Icarus*, *182*, 513–526.
- Smith, D. E., M. T. Zuber, and G. A. Neumann (2001), Seasonal variations of snow depth on Mars, *Science*, *294*, 2141–2146.
- Tapley, B. D., S. Bettadpur, M. Watkins, and C. Reigber (2004), The gravity recovery and climate experiment: Mission overview and early results, *Geophys. Res. Lett.*, *31*, L09607, doi:10.1029/2004GL019920.
- Vasavada, A. R., and A. P. Showman (2005), Jovian atmospheric dynamics: An update after Galileo and Cassini, *Rep. Prog. Phys.*, *68*, 1935–1996.

G. R. Flierl, Department of Earth, Atmospheric, and Planetary Sciences, Massachusetts Institute of Technology, 77 Massachusetts Ave., Cambridge, MA 02139, USA.

W. B. Hubbard and A. P. Showman, Lunar and Planetary Laboratory, University of Arizona, Kuiper Space Sciences Bldg., 1629 E. University Blvd., Tucson, AZ 85721-0092, USA.

Y. Kaspi, Division of Geological and Planetary Sciences, California Institute of Technology, MC 100-23, 1200 California Blvd., Pasadena, CA 91125, USA.